Experimental investigation of integrated radiant ceiling panel and diffuse ceiling ventilation under cooling conditions

Rugholm Krusaa, Marie; Ørduk Hoffmann, Ida; Anker Hviid, Christian

Published in:
Energy and Buildings

Link to article, DOI:
10.1016/j.enbuild.2022.112101

Publication date:
2022

Document Version
Publisher's PDF, also known as Version of record

Energy & Buildings 266 (2022) 112101

Contents lists available at ScienceDirect

Energy & Buildings

journal homepage: www.elsevier.com/locate/enb

Experimental investigation of integrated radiant ceiling panel and diffuse ceiling ventilation under cooling conditions

Marie Rugholm Krusaa [a,b,*], Ida Ørduk Hoffmann [a,b], Christian Anker Hviid [a]

[a] Technical University of Denmark, Department of Civil Engineering, Brovej, Building 118, DK-2800 Kgs. Lyngby, Denmark
[b] Saint-Gobain Nordic A/S, Robert Jacobsensvej 62A, 2300 København S, Denmark

ARTICLE INFO

Article history:
Received 17 October 2021
Revised 4 February 2022
Accepted 6 February 2022
Available online 16 April 2022

Keywords:
Heating
Cooling
Diffuse ventilation
Radiant ceilings
Heat transfer coefficient
Thermal comfort

ABSTRACT

This paper investigates experimentally the cooling performance of a concept, where the radiant ceiling is suspended from the hollow-core concrete slab and by ventilation supply in the plenum and the perforations of the ceiling tiles, ventilation air is distributed without ducts and air terminals to the occupied zone. Literature has proven that this concept allows for more streamlined installation procedures and excellent performance in terms of thermal comfort and draught. The paper reports experimental results from a climate chamber, where the concept was tested under both steady-state and quasi-steady conditions. The steady-state conditions were chosen to map the cooling performance with different air change rates, and different ventilation and water supply temperatures. The results showed that for air change rates of 3 h^{-1} in the occupied zone and water supply temperature of 17 °C, the cooling output from the ceiling increased by 10 %. The concept was also tested under quasi-steady conditions in a 48 h cycle to quantify the thermal buffering effect of the exposed upper concrete slab when subjected to ventilation supply air. The effect amounted to 11–12 % increased cooling capacity at the end of the working day when the driving temperatures between air, water and thermal zones were at their maximum.

1. Introduction

The increased focus on indoor thermal comfort has led to more extensive heating, cooling and ventilation demands. At the same time, there is a push to use more renewable energy sources for a greener and more sustainable environment [1]. Concurrently, the AEC industry (Architectural, Engineering and Contracting) seeks to simplify construction processes and reduce the coordination on the construction site. In buildings, the systems for heating, cooling, ventilation and acoustics belong to different professions, which increases the risk of sub-optimal performance or malfunction in one or more systems. This study presents a concept that integrates heating, cooling, ventilation and acoustics into one component to simplify the construction process and provide comfort and well-being more sustainably. The authors have presented the concept under the name 'HVACeiling' [2,3].

1.1. Integrated radiant and ventilative systems

The HVACeiling integrates a perforated radiant ceiling panel with Diffuse Ceiling Ventilation (DCV), which means the air flows from the distributing plenum to the occupied zone through the perforations of the panel at low speed, hence the term diffuse. In the literature, radiant ceilings and DCV have proven to improve thermal comfort [4,5] and reduce the risk of draught, respectively [6–8]. Using DCV for night ventilation shows to have a higher temperature efficiency than both displacement ventilation and mixing ventilation [9], however the temperature efficiency decreased for the DCV with higher ACR.

Fig. 1 exemplifies the concept in cooling and heating mode. The combination of radiant ceiling panels with diffuse ventilation builds upon the strengths of both solutions in terms of acoustics, draught, and the potential to use low-valued energy sources that provide heating and cooling at temperatures close to room comfort temperature. Previous studies have shown an increase in cooling power when integrating a hollow core concrete slab [2]. However, the heavy ceiling (concrete slab) is not an integral part of the system. The HVACeiling may be installed with a light ceiling, but in

* Corresponding author.
E-mail addresses: mrugholm@gmail.com, marrug@byg.dtu.dk (M. Rugholm Krusaa).

https://doi.org/10.1016/j.enbuild.2022.112101
0378-7788/

Nomenclature

A	Area [m^2]
ACR	Air change rate [h^{-1}]
AUST	Average Unheated Surface Temperature [K]
c_p	Specific heat capacity [J/kgK]
F	View factor [-]
h	Heat transfer coefficient [W/m^2K]
L	Length [m]
LMTD	Logarithmic Mean Temperature Difference [°C]
$\dot{m}$	Mass flow rate [kg/s]
Q	Heat gain/load/transfer [W]
ΔQ	Unbalance/deviation [W]
$\bar{Q}$	Unbalance rate [%]
q_i	Measured i^{th} quantity
q_{vent}	Ventilation rate [l/s]
n	Number of measurements
s	Standard deviation
T	Temperature [°C]
ΔT	Temperature difference [K]
U	U-value [W/m^2K]
u	Uncertainty [-]
V	Volume flow rate [m^3/s]

Greek symbols

ε	Emissivity [-]
ρ	Density [kg/m^3]
ψ	Linear loss [W/mK]

Abbreviations

CFD	Computer Fluid Dynamics
DCV	Diffuse Ceiling Ventilation
HVACeiling	Integrated Heating, Cooling, Ventilation and Acoustical ceiling solution
LTH-HTC	Low Temperature Heating – High Temperature Cooling
RTC	Reference Temperature Calibrator
TABS	Thermally Active Building Systems

Subscripts

a	Air
c	Convective
ceil	Ceiling
Cool	Cooling
op	Operative
out	Outside the climate chamber
plen	Plenum
room	Room
r	Radiant
ref	Reference
ret	Return
s	Surface
sup	Supply
tot	Total
vent	Ventilation
w	Water

this paper, the HVACeiling was tested in combination with a hollow core concrete slab.

Systems operating with temperatures close to the room comfort temperature are commonly referred to as Low-Temperature-Heating - High-Temperature-Cooling systems (LTH-HTC) [5]; and are regarded as more sustainable providers of comfort. Radiant ceilings can be operated as LTH-HTC systems, provided that the heat transfer surface is sufficiently large to supply heating and cooling to the room at low temperature differences. Other types of LTH-HTC ceilings encompass systems embedded in the primary structure (thermo-active building systems, TABS), systems isolated from the main structure but embedded in the outermost surface layer, and systems suspended from the main structure [10,11].

Fan coils and chilled beams are other examples of integrated heating, cooling and ventilation systems. However, these systems are often sources of turbulent noise, draught and discomfort [12] and in heating scenarios often require pre-heating of the supply air to minimise discomfort risks. The presented concept here allows the ventilation air to diffuse through the perforations at slow speed, in the process pre-heating or pre-cooling the supply air and thus is an integrated solution for draught risk, turbulent noise and room acoustics. Some recent studies have combined Active Chilled Beam (ACB) with LTH-HTC systems [13]. In [13], the ACB operated with a constant water supply temperature and by induction and recirculation cooling and heating was transferred from water to the room air [14]. However, in comparison with DCV, the ACB operates with high-impulse airflow which increases the risk of draught and turbulent noise. This was shown by Lestinen et al. [4], where maximum draught rates of chilled ceiling with mixing ventilation, diffuse ceiling ventilation and chilled beams were 16, 19 and 21 %, respectively, at approx. 60 W/m^2. Taking into consideration that the air change rate with diffuse ventilation was 5.9 h^{-1} and only 1.9 h^{-1} in the other cases, the DCV draught performance was superior.

Previous studies of Diffuse Ceiling Ventilation (DCV) combined with hydronic radiant ceilings showed a great potential [2,15–18]. Integrated heating, cooling, ventilation and acoustics were analysed by Yu et al. [15], Zhang et al. [16,17] and Krusaa et al. [2,3,18]. Yu and Zhang performed analyses of TABS combined with DCV and compared the radiant heat exchanger with and without a

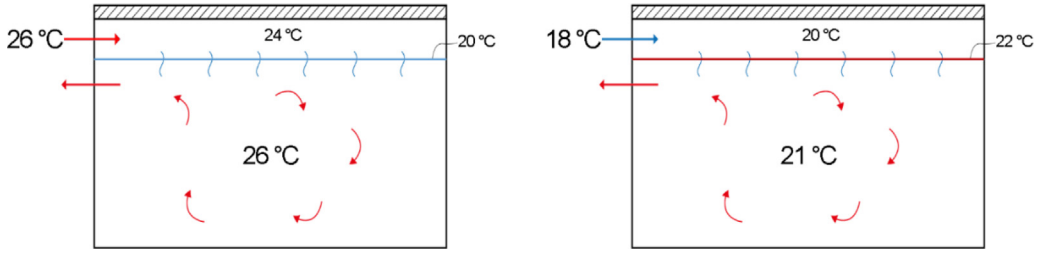

Fig. 1. The HVACeiling concept [2]. Ventilation supply to plenum and extract from room. Left: cooling mode. Right: heating mode.

suspended acoustic ceiling. As the suspended ceiling blocks the radiant heat transfer to the room, these studies showed decreased cooling capacity. The decrease in cooling capacity was expected as Langner et al. [19] found that the heat transfer for TABS reduces significantly when the suspended ceiling covers>60 % of the ceiling. Krusaa et al. [2] performed analyses of DCV with a radiant ceiling suspended from the building structure, including the influence of the concrete slab on the pre-heat/pre-cooling scheme. The combined ceiling solution showed an increase of up to 16 % with an exposed slab, compared to the reference scenario with a radiant ceiling and mixing ventilation.

There exist some patents that outline a concept similar to HVACeiling. One patent from 1955 described perforated metal plates prepared for diffuse ventilation exposed to suspended pipes during assembly [20]. Another patent from 2008 introduced a composite, hybrid radiant multi-role panel with forced and natural convection [21]. This panel integrated heating, cooling, ventilation and air conditioning, as well as a thermoelectric effect, energy recovery and thermal storage functionalities. Performance analyses back neither combination patents; however, some combined systems are being marketed [22]. These solutions are designed with suspended canopies and impulse systems to recirculate the room air to the backside of the canopy to reduce the boundary layer and add maximum convection to the radiant ceiling. One solution combining TABS with a partly covered ceiling with acoustics panels up to 62 % showed a decrease in the cooling capacity of 17 % initially, but by introducing ceiling fans, the decrease turned to an overall increase of 9 % [23,24]. However, ceiling fans and high-impulse solutions may cause unwanted draught and turbulent noise. Other solutions are being marketed where high-impulse jet systems reduce the boundary layer by design, thus increasing the convective heat transfer [25].

1.2. Aims of current research

The HVACeiling concept is promising because it simplifies the construction process. Simulations have indicated positive influence from the thermal mass of the concrete slab in the plenum, and the literature review showed that individual elements of the concept have proven beneficial, e.g. in terms of draught, thermal comfort, acoustics, and the possibility of integrating a larger share of renewable energy sources. However, experimental evidence of the performance of the combined solution is necessary. This study aims to investigate the integrated solution in a full-scale experimental setup with a particular focus on both the combined and the convective heat transfer coefficients and the cooling performance. The performance was mapped with different water temperatures and ceiling crossing airflows of different magnitudes. Mixing scenarios, i.e. without DCV but with air supplied directly to the occupied zone, were investigated for comparison. The investigations were made under steady-state and quasi-steady-state conditions.

The first working hypothesis stipulates that the integrated HVACeiling solution has higher cooling performance with diffuse ventilation in steady-state conditions because cooling that is otherwise lost to the plenum is "reused" to pre-cool the ventilation air. The heat transfer coefficients upward and downward from the ceiling and downward from the slab in the plenum were measured to map the effective heat transfer coefficients. This mapping of the heat transfer coefficient can be used for further investigation in simulation tools to achieve more accurate simulations for radiant ceilings combined with diffuse ventilation. Experiments are steady-state, meaning that the influence of the slab is nullified. This nullification may introduce a significant error because the slab can never be in balance in a 24 h cycle. For this reason, also quasi-steady experiments are setup to explore how much energy can be saved/shifted from day to night.

Thus the second working hypothesis stipulates: using diffuse ventilation instead of mixing ventilation means that stored cooling (from circulation at night) in the top slab is more usable (cooling power is higher for equal ventilation rates) because the heat exchange from the slab to the ceiling and on to the occupied zone is increased by higher convective heat transfer.

1.3. Novelty

The novelty of this study is experimental verification of previous numerical studies showing that the combination should 1) potentially increase the cooling capacity, 2) improve storage of heat energy in a heavy slab in the plenum and 3) provide adequate thermal comfort by a combination of 1 and 2 at high water supply temperature close to room temperature which is a more sustainable solution.

2. Experimental setup

The experimental investigations were conducted using the test facilities in the laboratory hall. The hall had a relatively constant temperature of 20–23 °C. The test facilities consisted of a climate chamber placed inside a temperature-guarded box, as shown in Fig. 2. The climate chamber was the size of a full-scale reference office, 6 m long and 3.6 m wide, with a room height of 2.85 m from the floor to the lower edge of the suspended ceiling. The plenum height was 0.6 m. The climate chamber top and bottom were made from hollow-core slabs, and the walls were made from plasterboards insulated with 100 mm insulation.

The airflow and water flow rates varied for the experimental investigations, whereas heat gains were fixed. The occupants' heat gain came from three thermal dummies, resulting in 7 m^2/person (330 W) and three thermal dummies for 7 W/m2 (150 W) equipment. In addition, windows, the size of 3.2 × 1.6 m, were emulated with a heat resistant film on the wall. The windows resulted in a heat gain of 450 W, assuming solar-coated glazing with a g-value of 0.31. The solar gain was placed on the wall and not the floor because the solar coating and a glare screen (expected to be activated during direct sun) would absorb the radiation. Therefore, the total heat gain applied to the room was 930 W (43 W/m^2).

The suspended ceiling used for the experiments were ceiling tiles from Climaline GmbH [26], type *Thermo Panel 4 T* (c.f. Fig. 3). The tiles were 600 × 600 mm and were built up from the front to the back with:

- A perforated gypsum board, 6.5 mm thick and with perforation holes of 9x9 mm, resulting in 9 % perforation, including the blocked area. The gypsum was mixed with graphite to improve the thermal conductivity to 0.45 W/mK.
- An acoustic felt
- A heat-conducting metal plate (1 mm) with matching perforation pattern, colour black
- Meandering cobber pipes (12 × 0.35 mm) mounted by four aluminium plates with a centre to centre distance of 150 mm

The ceiling tiles were placed in three circuits of 15 tiles, as shown in Fig. 4, resulting in a coverage factor of 75 % in the room. Each circuit was connected to the manifold and supplied with water from a cooling rack. Each circuit had a water flow of approx. 100 kg/h (ceiling total 300 kg/h), which caused a pressure loss of 280 Pa/m, which was well within the design criteria for the system. Infrared thermography of the ceiling verified that water distribution was uniform (Fig. 5, b). Reynolds number for each circuit was 3123 which indicates mixed turbulent and laminar flow.

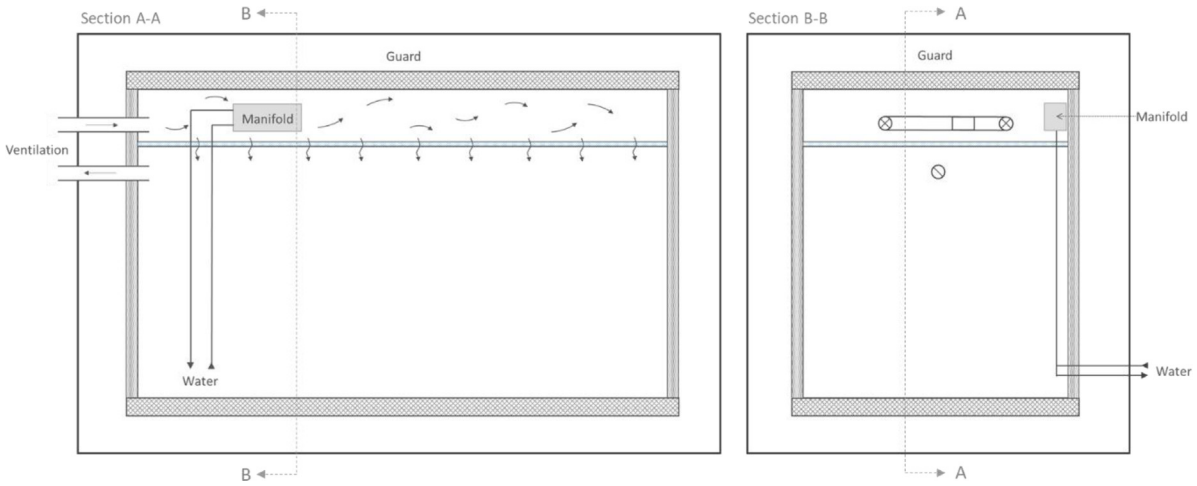

Fig. 2. Cross-sections of the test facilities with climate chamber inside the temperature-guarded box, including ventilation inlet for diffuse ceiling ventilation and water supply/return to the manifold.

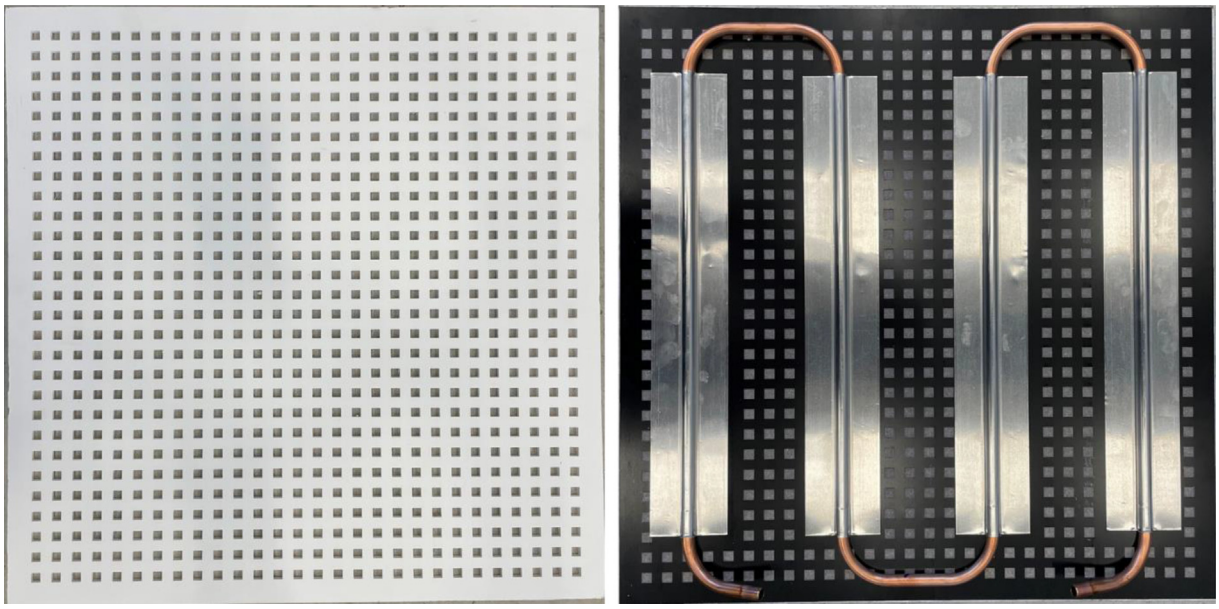

Fig. 3. Thermo Panel 4 T front (left) and backside (right) of the ceiling tiles used for the experiment.

The diffuse ceiling ventilation principle supplies air above the suspended ceiling end extracts air directly from the room below. The principle is depicted in Fig. 2. The ventilation inlet was split in two to get a more uniform air distribution, uniform velocity profile and reduce dynamic pressure differences in the plenum. The radiant ceiling was also tested with ventilation supply directly to the room to make a fair comparison of the HVACeiling solution. The ventilation principle was made by diverging the supply air through the ceiling with a flex duct going down in the room. A board was placed a few centimeters in front of the duct to prevent a jet of air in the lower part of the room. The principle was similar to a low-momentum air diffuser that relies on the buoyant forces to move the air. But in combination with the chilled ceiling, the anticipated air pattern would - according to Rehva Guidebook 01 [27] - resemble mixing and these scenarios were therefore dubbed "mixing".

The ventilation rates corresponded to Category I and II from DS/ISO/TR 17772–2 [28], resulting in ventilation rates of 51.6 l/s (2.4 l/s per m^2 and 3 h^{-1} in the room) and 36.1 l/s (1.5 l/s per m^2 and 2 h^{-1} in the room). An overview of the different experiments can be found in Table 1, and pictures of the experimental setup can be found in Fig. 5.

2.1. Experimental scenarios

Two different kinds of experiments for each of the ventilation principles were conducted.

1. Steady-state had the experiments running for 24 h. Average values of the last hour (360 samples) were used for reporting.
2. Quasi-steady-state, where the experiments were running 48–72 h. Values from the last 24 h (8640 samples) were used for reporting. Quasi-steady experiments test the potential thermal buffering capacity of the hollow-core concrete slab.

The different scenarios were set up with three water temperatures and two different air change rates per hour (ACR), totalling 21 experiments. All of the tested scenarios and naming conven-

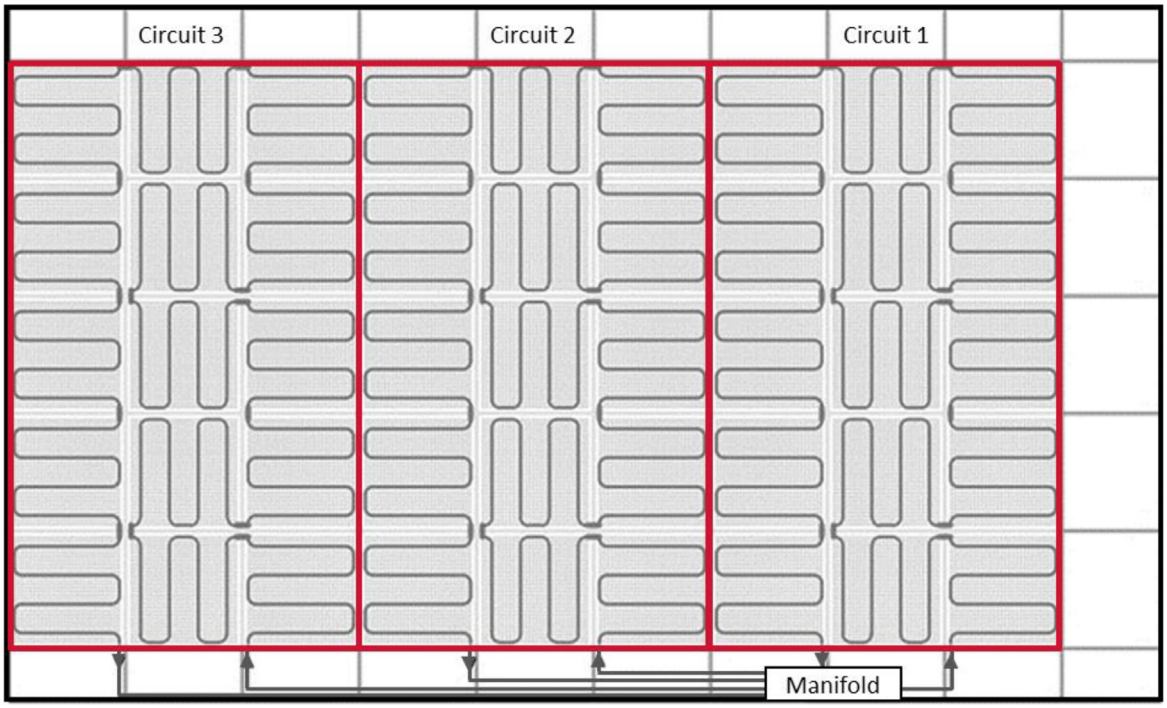

Fig. 4. The layout of ceiling tiles and connection to the manifold.

tions are found in Table 1. The final operative temperature, heating of water and thermal balances could not be known prior to the experiments, but for illustration, a target operative temperature of 26 °C, water supply temperature of 20 °C and air supply temperature of 23 °C would result in water cooling output of 1045 W and ventilation cooling output of 130 W to 187 W for the two air changes.

2.2. Measuring equipment

Several physical parameters and energy use were measured and recorded. The test facilities were equipped with 45 measurement points with thermocouples to measure surface and air temperatures, thermopiles to measure the temperature difference, heat flux sensors to measure the heat flux from the surface, flow meter and micro-manometer to measure water and airflow. The measurement equipment is listed with accuracy and interval in Table 2. The location of each measuring point can be found in Fig. 6. A column of thermocouples was placed at a central location in the room, following DS/EN 16798–3 [29], to determine the vertical air temperature gradient and evaluate the effect of thermal stratification based on the experimental scenarios. The thermocouples were placed at the following heights from the floor: 0.1 m (ankle of the occupant), 0.6 m (the core of sedentary occupant), 1.1 m (neck of the sedentary occupant), 1.7 m (neck of the standing occupant), 2.1 m, 2.5 m and 2.8 m.

The internal heat gain (electricity) was measured with multimeters as listed in Table 2. The final gain stabilized during the experiment as resistances and temperatures reached the state of equilibrium. The reported value was measured at the end of each experiment.

2.2.1. Calibration of equipment

All thermocouples were covered with aluminium tape or placed inside a short aluminium tube with open ends to protect the thermocouples from ambient radiant influence. The sensors measuring water temperature were placed in a thermowell, in direct contact with the water flow. Both thermocouples and thermopiles measured the water temperature as the thermopiles measuring the temperature difference is more accurate. To ensure each thermocouple measuring data, they were all calibrated with the Reference Temperature Calibrator (RTC) from Ametek, ATC-155B, which has an accuracy of 0.03 °C. The thermocouples in the guard were not accessible, but all other thermocouples were calibrated, which means the accuracy of the temperature readings are on par with the accuracy of the Ametek RTC. The max deviation for the thermocouples was ± 1 °C from the reference value.

PT100 sensors measured operative temperature in the room (placed 1.1 m from the floor) and in the middle of the plenum. The sensors were placed within a grey globe, 40 mm in diameter. The sensor is influenced by air- and mean radiant temperature as a standing person would be and therefore applicable for measuring operative temperatures [31]. The cable length connected to the PT100 sensors influences the calibration. Therefore the cable and PT100 sensor was assembled prior to the calibration with the Ametek RTC.

The inlet and outlet airflows were measured with pitot tubes from Veab AB with a diameter of Ø160 on the inlet and outlet. The ventilation rate was not logged continuously during the experiment. The ventilation rate fluctuations were monitored manually (±1 %), and deemed within the accuracy of the measurement tool (±5 %).

The heat flux sensors (HF-10S from EKO, [32]) were carefully attached with no air gaps on surfaces with thermally conductive silicone grease (Electrotube, HTS [33]). The heat flux sensors measured the combined radiant and convective heat flux from the surface at the exact location of the sensor. The sensors were placed on both sides of the ceiling tile and the slab in the plenum. The sensors' placement was on Circuit 2 and Circuit 3 (c.f. Fig. 4), approximately 1/3 from the manifold downstream, as this location represents the driving temperature gradient better.

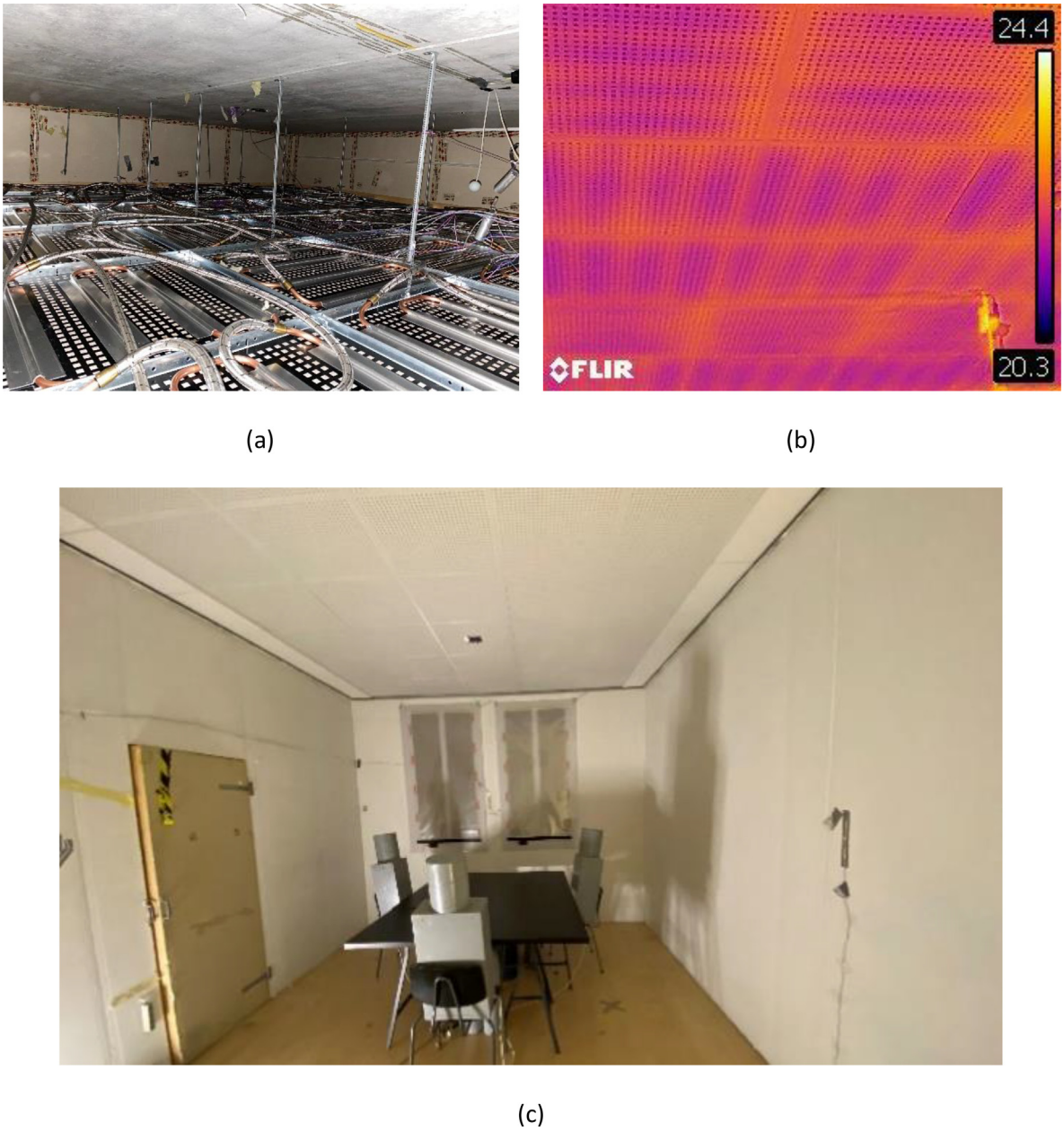

Fig. 5. Experimental setup in the climate chamber for a) integrated solution seen from plenum with connections between each ceiling tile, b) infrared thermography of the ceiling and c) diffuse ceiling setup from the room.

Table 1
Experimental scenarios. Cooling demand, air temperature and water flow were kept constant, so only ACR and water supply temperature was changed.

	Cooling demand	ACR [h^{-1}]	Air supply temperature [°C]	Water temperature [°C]	Steady-state	Quasi-steady state
Diffuse	930 W 43 W/m^2	2	23	17	D.2.17	D.Q.2.17
			23	20	D.2.20	D.Q.2.20
			23	23	D.2.23	D.Q.2.23
		3	23	17	D.3.17	D.Q.3.17
			23	20	D.3.20	D.Q.3.20
			23	23	D.3.23	D.Q.3.23
Mixing		2	23	17	M.2.17	–
			23	20	M.2.20	–
			23	23	M.2.23	–
		3	23	17	M.3.17	M.Q.3.17
			23	20	M.3.20	M.Q.3.20
			23	23	M.3.23	M.Q.3.23

Table 2
Accuracy of instruments and sensors applied in the experimental setup.

Instrument/sensor	Purpose	Interval	Accuracy
Thermocouples	Temperature	−75 to + 260 °C	± 0.03 °C[1]
Thermopiles	Temperature	−270C to + 370 °C	± 0.009 °C[2]
PT-100 sensor	Temperature	−50 to + 500C	± 0.03 °C[1]
Keysight 34,970 data acquisition	Data logger	−210 to + 1820 °C	± 0.003 +0.0035 %
Furness FC0510 micromanometer	Differential pressures	0 to 2000 Pa	± 0.25 %
HF-10S heat flux sensor	Heat fluxes	−30 to + 120C	± 2 %
MASSFLO Flowmeter type MASS 1100	Mass flow	0 to 2200 kg/h −50 to + 180C	± 0.1 %
Veab measuring tube Ø160	Airflow	38 to 130 l/s	± 5 %
Multimeter UNI-R UT33D	Volt/Ampere	0 to 500 V	± 2.2 %
Multimeter	Volt/Ampere	0 to 200 A	± 1.6 %

[1] Based on accuracy of Reference Temperature Calibrator from Ametek ATC-155B. Mean of three-point (at 10, 20, 30 °C) calibration offset was applied to average of sample readings (360) from sensors
[2] Based on [30]

3. Analytic criteria

3.1. Energy balance

The energy balance for the steady-state experiments was expressed by equation (1). Where ΔQ indicated the unaccounted deviation in the energy balance, some deviations were due to uncertainties in the measurements as described in section 3.3. The unbalance rate $\bar{Q}$ was defined by equation (2).

$$\dot{Q}_{air} + \dot{Q}_{water} + \dot{Q}_{transmission} + \dot{Q}_{internalgain} = \Delta\dot{Q} \quad (1)$$

$$\bar{Q} = \frac{\Delta\dot{Q}}{\dot{Q}_{internalgain}} \quad (2)$$

The ventilation heat gain/loss was defined by equation (3), and the water heat gain/loss was defined by equation (4). The cooling capacity was calculated by equation (5).

$$\dot{Q}_{air} = \dot{V} \cdot \rho_a \cdot c_{p,a} \cdot (T_{a,sup} - T_{a,ret}) \quad (3)$$

$$\dot{Q}_{water} = \dot{m} \cdot c_{p,w} \cdot \Delta T_w \quad (4)$$

$$\dot{Q}_{cool} = \frac{\dot{Q}_w}{A} \quad (5)$$

The transmission loss (Equation (6)) was based on the U-values, and linear losses from a previous study by Onsberg and Eriksen [34] and was separated into two parts, plenum and room. The U-value of the plenum included the top slab (2.15 W/m^{2}K) and the

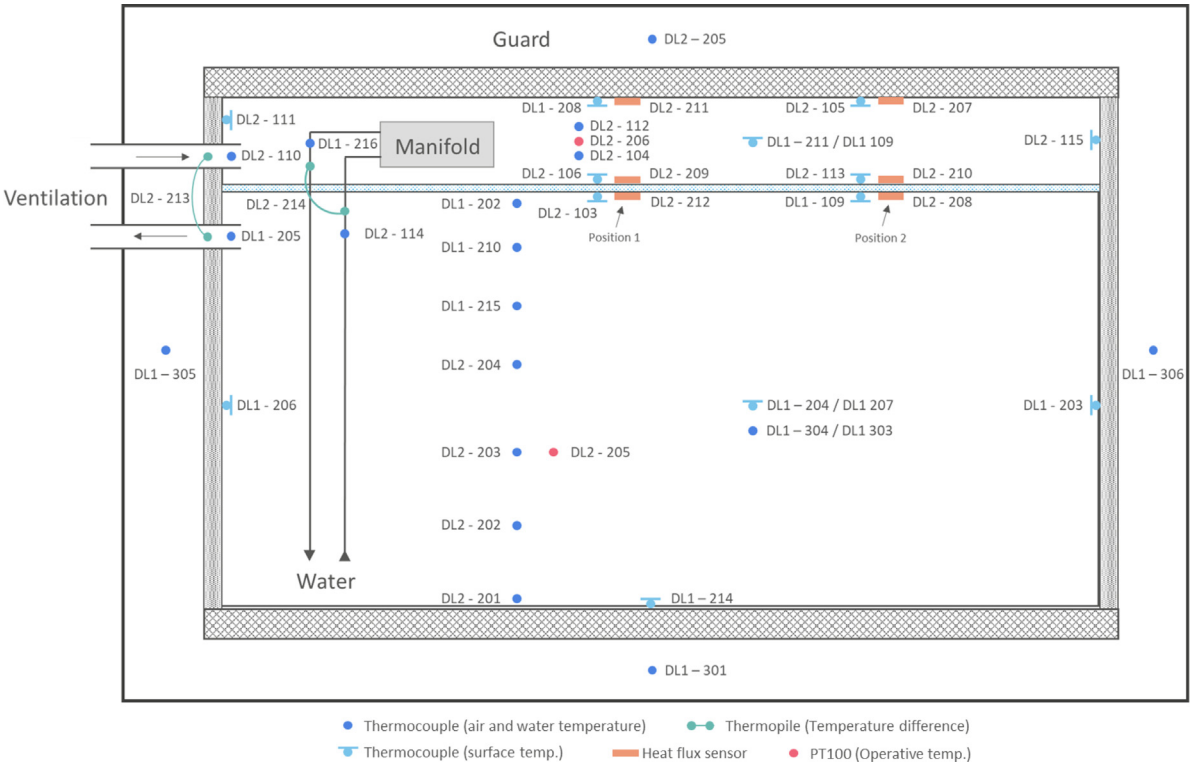

Fig. 6. Measurements points in the experimental setup. Position 1 and 2 indicate the placement of the heat flux sensors for use in the results.

walls (0.38 W/m^{2}K). The room included the floor slab (1.32 W/m^{2}K) and the walls. A linear loss of 0.15 W/mK is included for each corner side and the connection between floor/wall and ceiling/wall.

$$\dot{Q}_{transmission} = \sum \left(U_{s,plen} \cdot A_{s,plen} + \Psi \cdot L_{plen}\right) \cdot \left(T_{a,plen} - T_{a,out}\right) + \sum \left(U_{s,room} \cdot A_{s,room} + +\Psi \cdot L_{room}\right) \cdot \left(T_{a,room} - T_{a,out}\right) \quad (6)$$

3.2. Heat transfer coefficients

The heat transfer coefficients are essential for dimensioning radiant systems and numerical simulations, CFD analyses and load calculations. Simulation software uses either 'hardcoded' values or simulates the values during runtime for the Radiative (RHTC) and Convective Heat Transfer Coefficient (CHTC), and often radiant and convective heat transfer coefficients are lumped together to form the combined heat transfer coefficient [35]. The heat transfer coefficients are greatly influenced by the ventilation in a room, as the ventilation changes the boundary layer close to the surfaces of the radiant comfort systems [5,36,37]. The heat transfer coefficients are also dependent on the chosen reference temperature, which again depends on the temperature uniformity in the room [38,39]. The literature outlines several equations and values with different reference temperatures for calculating the heat transfer coefficient. The total heat transfer coefficient is often reported regarding the operative temperature [40–46]. The radiant heat transfer coefficient refers to the radiant heat exchange with the surroundings, driven by the radiant surface temperature to the surroundings' Average Unheated Surface Temperature (AUST). The convective heat transfer is driven by the temperature difference between surface and room air [47].

In this study, the airflow patterns at the suspended ceiling surfaces in the room and the plenum and at the top slab may be very complex. Therefore, the convective heat transfer coefficient was derived from the total heat transfer coefficient and the calculated radiant heat transfer coefficient. The radiant heat transfer coefficient refers to the radiant heat exchange with other surfaces, driven by the surface temperature and the mean radiant temperature of the surroundings. The convective heat transfer is driven by the temperature difference between surface and bulk room air. The heat flux sensor measured the total heat transfer coefficient, the combined heat transfer for radiation and convection during the experiment. The total heat transfer coefficient h was calculated as equation (7), where the driving temperature gradient was the surface temperature and the operative temperature.

$$h_{tot} = \frac{\dot{Q}_{tot}/A}{(T_{op} - T_s)} \quad (7)$$

The radiant heat transfer coefficients (h_r) was derived from the calculation of averaged unheated surface temperature (AUST), including the view factors in equation (8)-(11). The emissivity, ε_s, of the radiant ceiling in the plenum is 0.6, as the heat distribution plates were of polished aluminium and covered 38 % of the ceiling tiles. All other surfaces were 0.9; the actual view factors can be found in Table 3. The radiant heat transfer coefficient was calculated by Equation (12).

$$AUST = \sqrt[4]{\sum_{j=1}^{n} F_{s-j} T_j^4} \quad (8)$$

$$F_{s-j} = \frac{1}{A_i} \int_{A_i} \int_{A_j} \frac{\cos\theta_i \cos\theta_j}{\pi R^2} dA_i dA_j \quad (9)$$

$$F_{\varepsilon_{s-j}} = \frac{1}{((1-\varepsilon_s)/\varepsilon_s) + (1/F_{s-j}) + (A_s/A_j)((1-\varepsilon_j)/\varepsilon_j)} \quad (10)$$

$$\dot{Q}_r/A = \sum_{j=1}^{n} \sigma F_{\varepsilon_{s-j}} \left[(T_j + 273.15)^4 - (T_s + 273.15)^4\right] \quad (11)$$

$$h_r = \frac{\dot{Q}_r/A}{(AUST - T_s)} \quad (12)$$

The convective heat flux due to the heated/cooled ceiling [35] were calculated by subtracting the radiant heat flux from the total heat flux:

$$\frac{\dot{Q}_c}{A} = \frac{\dot{Q}_{tot}}{A} - \frac{\dot{Q}_r}{A} \quad (13)$$

The convective heat transfer coefficient based on air temperature was then calculated from:

$$h_c = \frac{\dot{Q}_c/A}{(T_a - T_s)} \quad (14)$$

The local heat transfer coefficients derived from the heat flux sensors mounted on the suspended ceiling and the slab, were influenced by thermal phenomena and the local airflow patterns. To calculate the global heat transfer coefficient by the water heat transfer is a more robust method to derive the heat transfer from the HVACeiling to the room. Equation (15) uses the surface temperature and the operative temperature, where equation (17) uses the logarithmic mean temperature difference (LMTD).

$$h_{global} = \frac{\dot{Q}_w}{A(T_s - T_{op})} \quad (15)$$

$$LMTD = \frac{T_{w,sup} - T_{w,ret}}{\ln\left((T_{w,sup} - T_{op})/(T_{w,ret} - T_{op})\right)} \quad (16)$$

$$h_{LMTD} = \frac{\dot{Q}_w}{A \cdot LMTD} \quad (17)$$

3.3. Uncertainty analyses

As part of the validation process, all reported results have undergone uncertainty analysis [48], which includes the accuracy and precision of the experiments. The accuracy is the proximity of the measured value to the true value, while precision refers to the closeness of repetitively measured values. The first part of the uncertainty analysis contains the standard deviation, s (equation (18)) and the estimated standard uncertainty, u (equation (19)). The standard deviation, x_i is the measured i^{th} value, $\bar{x}$ is the average value of all the measurements, and n is the number of measurements.

$$s = \sqrt{\frac{\sum_{i=1}^{n} \left(x_i - \bar{x}\right)^2}{(n-1)}} \quad (18)$$

Table 3
View factors, F, from the radiant ceiling.

	Plenum	Room
Slab/Floor	0.78	0.34
Wall (Long side)	0.07	0.21
Wall (Short side)	0.04	0.12

$$u = \frac{s}{\sqrt{n}} \tag{19}$$

From the calculation, it is essential to find the combined uncertainty (equation (20)) for each parameter, including the uncertainty of the measuring equipment (Table 2). From this combined uncertainty, it is possible to estimate uncertainty for an equation, e.g. to find the uncertainty of the entire energy balance. Here it is essential to use equation (20) and (21). Equation (20) also describes the uncertainty when two parameters are added or subtracted, and equation (21) describes when parameters are multiplied or divided.

$$\boldsymbol{Combineduncertainty} = \sqrt{a^2 + b^2 + c^2 + \cdots etc}. \tag{20}$$

$$\frac{u(x)}{|x|} = \sqrt{\frac{u(y)^2}{|y|} + \frac{u(z)^2}{|z|} + \cdots etc}. \tag{21}$$

4. Results

The results from the 21 experiments (12 steady-state and 9 quasi-steady-state) are presented in the following section. The reported results for the steady-state experiments are the average of the last hour of the experiment: 360 recordings. The steady-state experiments were running untouched for at least 24 h to achieve steady-state. Uncertainty analyses were conducted for both the energy balance and the heat transfer coefficients, including the standard deviation of the 360 recordings and the accuracy of the measuring equipment. The sign convection for heating was positive and negative for cooling, except for the heat transfer coefficients, which were positive in all cases. The results for the quasi-steady-state were evaluated from the last 8640 measurements, which corresponded with 24 h. Time series are reported to show the variations over a day, e.g. when the workday starts and ends.

4.1. Steady-state

The results were analysed based on the measured values. Table 4 shows the values for all steady-state scenarios. Thermal comfort was evaluated by operative temperature and vertical temperature gradient. From Table 4, it can be seen that the water temperature of 23 °C was not sufficient to create acceptable operative temperature ($T_{op,room}$), in regards to the temperature criteria from DS/EN 17772–2, which states that the temperature should be below 25.5 °C for category I and below 26.0 °C for category II. Using a water temperature of 20 °C ensures thermal comfort category II and 17 °C ensures category I. The operative temperature in the room is slightly higher than the air temperature ($T_{op,room} > T_{a,room,1.1}$); an explanation for this is offered in the Discussion, section 5.3.

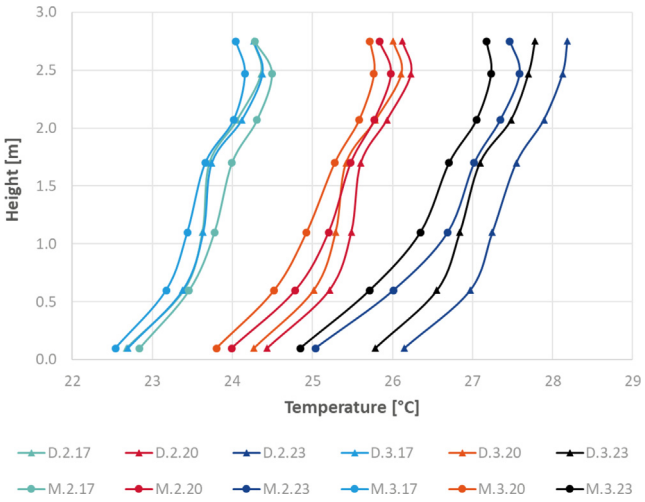

Fig. 7. The vertical temperature gradient from the steady-state experiments.

The vertical temperature gradient through the room is shown in Fig. 7. According to ISO 17772–1 [49], the acceptable vertical temperature gradient in category I is 2 °C from head (1.1 m) to ankles (0.1 m). Whenever there is a significant temperature difference, the occupants feel discomfort. The temperature gradients were for the diffuse cases in the range 0.9–1.1 °C where the mixing cases were in the range of 0.9–1.7 °C, rising with warmer water supply temperature, but was largely unaffected by the ventilation method. This is indirect evidence that the air patterns were similar. This is discussed in Section 5.1.

The energy balance for the steady-state scenarios are shown in Table 5, where the unbalance, unbalance rate, and uncertainty is reported. The unbalance rate is low for all cases, and the uncertainty can explain most of the unbalance. The unbalance of the cases with a water temperature of 20 °C was highest, as the plenum, slab, and floor became almost adiabatic with very small temperature differences, and therefore the uncertainty of the measurements was high. As an example, for Case M.3.20, the uncertainty is approx. ± 137 W, since the temperature difference between the plenum and guard is only 0.07 °C, which causes con-

Table 4
Measured temperatures, water flow and airflow rate from the steady-state experiments.

		D.2.17	D.2.20	D.2.23	D.3.17	D.3.20	D.3.23	M.2.17	M.2.20	M.2.23	M.3.17	M.3.20	M.3.23
$T_{s,ceil,plen,1}$	[°C]	19.4	22.2	24.9	19.7	22.2	24.6	19.3	22.2	24.7	19.4	22.4	24.6
$T_{s,ceil,plen,2}$	[°C]	19.1	21.8	24.5	19.5	21.9	24.3	19.2	21.9	24.3	19.2	22.1	24.4
$T_{s,ceil,room,1}$	[°C]	20.3	23.0	25.6	20.6	22.9	25.3	20.3	22.9	25.4	20.3	23.1	25.3
$T_{s,ceil,room,2}$	[°C]	20.2	22.8	25.4	20.5	22.8	25.1	20.4	22.8	25.1	20.3	23.0	25.2
$T_{s,slab,plen,1}$	[°C]	21.1	22.2	24.0	21.0	22.4	24.0	20.7	22.3	23.4	20.7	21.9	24.1
$T_{s,slab,plen,2}$	[°C]	21.0	22.2	24.1	21.0	22.4	24.1	20.7	22.3	23.5	20.7	21.9	24.2
$T_{a,plen}$	[°C]	20.8	22.2	23.9	20.9	22.3	23.8	20.5	22.3	23.8	20.5	22.1	24.2
$T_{a,room,1.1}$	[°C]	23.6	25.5	27.2	23.6	25.3	26.8	23.8	25.2	26.7	23.4	25.3	26.7
$T_{op,plen}$	[°C]	21.1	22.4	24.2	21.2	22.5	24.2	20.7	22.5	24.1	20.7	22.3	24.4
$T_{op,room}$	[°C]	24.3	26.1	28.1	24.3	25.9	27.8	24.5	26.0	27.6	24.2	25.7	27.2
T_{guard}	[°C]	22.1	22.6	23.4	22.1	22.7	23.5	21.8	22.3	22.7	21.8	22.2	23.0
$T_{water,sup}$	[°C]	17.0	20.2	23.2	17.5	20.2	23.0	17.1	20.3	23.3	17.1	20.7	23.2
ΔT_{water}	[°C]	−2.3	−1.7	−1.2	−2.2	−1.7	−1.2	−2.1	−1.5	−1.1	−2.0	−1.3	−1.1
$T_{vent,sup}$	[°C]	22.8	23.0	22.8	22.6	23.0	22.8	22.2	22.1	22.1	22.1	22.1	22.2
ΔT_{vent}	[°C]	−1.7	−3.3	−5.6	−1.9	−3.1	−5.1	−2.5	−4.2	−6.0	−2.3	−4.0	−5.3
$\dot{m}$	[kg/s]	0.086	0.081	0.083	0.085	0.079	0.083	0.086	0.086	0.085	0.085	0.085	0.084
q_{vent}	[l/s]	36.0	36.0	36.0	51.6	51.6	51.6	36.0	36.0	36.0	51.6	51.6	51.6

Table 5
Energy balance of the experiment from measured values.

		D.2.17	D.2.20	D.2.23	D.3.17	D.3.20	D.3.23	M.2.17	M.2.20	M.2.23	M.3.17	M.3.20	M.3.23
$Q_{internal\ gains}$	[W]	935.6	932.0	919.4	932.0	932.0	917.1	938.9	926.2	928.0	938.9	932.0	951.7
Q_{water}	[W]	−813.5	−579.2	−399.8	−771.4	−576.4	−391.9	−760.5	−549.6	−373.3	−729.5	−470.8	−398.9
Q_{air}	[W]	−73.2	−143.4	−242.2	−120.4	−190.3	−320.0	−107.7	−182.0	−262.2	−144.4	−251.7	−331.6
$Q_{transmission}$	[W]	−65.8	−181.3	−295.0	−71.6	−163.8	−266.8	−88.7	−208.5	−333.7	−66.9	−191.6	−296.8
ΔQ	[W]	−16.9	28.1	−17.6	−31.4	1.5	−61.7	−18.0	−13.9	−41.3	−1.9	17.9	−75.6
$\bar{Q}$	[%]	−1.8	3.0	−1.9	−3.4	0.2	−6.7	−1.9	−1.5	−4.4	−0.2	1.9	−7.9
Uncertainty	[W]	± 26.5	± 56.6	± 36.0	± 27.3	± 49.4	± 39.1	± 27.3	± 56.0	± 34.1	± 27.9	±137.8	± 36.7

Table 6
The total, radiant and convective heat transfer in plenum and room for diffuse ventilation scenarios. Position 1 and 2 refers to the heat flux sensor positions in Fig. 6.

		D.2.17		D.2.20		D.2.23		D.3.17		D.3.20		D.3.23	
	Position	1	2	1	2	1	2	1	2	1	2	1	2
$Q_{tot,slab}/A$	[W/m^2]	−3.0	−2.7	−0.6	−1.0	−2.1	−2.4	−2.2	−1.9	−0.3	0.0	−0.7	−1.0
$Q_{tot,plen}/A$	[W/m^2]	−12.2	−9.0	−3.8	−2.3	1.5	2.1	−10.7	−7.8	−5.2	−3.8	0.4	1.0
$Q_{tot,room}/A$	[W/m^2]	−38.1	−47.8	−31.4	−41.1	−26.6	−35.8	−35.4	−45.2	−30.2	−39.5	−25.4	−34.3
$Q_{r,plen}/A$	[W/m^2]	−8.5	−9.8	−0.1	−1.9	4.3	2.6	−6.6	−7.7	−1.2	−2.6	3.1	1.6
$Q_{r,room}/A$	[W/m^2]	−20.4	−21.3	−14.9	−16.1	−10.6	−12.0	−18.8	−19.7	−15.1	−15.7	−10.4	−11.6
$Q_{c,plen}/A$	[W/m^2]	−3.7	0.8	−3.7	−0.4	−2.8	−0.6	−4.1	−0.1	−4.0	−1.1	−2.7	−0.5
$Q_{c,room}/A$	[W/m^2]	−17.8	−26.2	−16.5	−25.0	−15.9	−23.8	−16.6	−25.5	−15.1	−23.7	−14.9	−22.7
$AUST_{plen}$		21.1	21.1	22.2	22.2	24.0	24.0	21.1	21.1	22.4	22.4	24.0	24.0
$AUST_{room}$		24.0	24.0	25.7	25.7	27.5	27.5	24.0	24.0	25.6	25.6	27.1	27.1
$h_{tot,slab}$	[W/m^{2}K]	57.9	34.2	2.8	4.3	10.1	20.0	14.0	11.0	4.3	0.1	5.7	22.1
$h_{tot,plen}$	[W/m^{2}K]	7.0	4.5	21.2	4.4	2.3	6.3	7.4	4.7	17.9	6.6	0.9	7.4
$h_{tot,room}$	[W/m^{2}K]	9.6	11.5	10.0	12.3	10.6	13.1	9.5	11.7	10.0	12.5	10.3	12.8
$h_{r,plen}$	[W/m^{2}K]	4.0	4.0	4.4	4.4	4.1	4.1	4.0	4.0	4.1	4.1	4.3	4.3
$h_{r,room}$	[W/m^{2}K]	5.5	5.5	5.6	5.6	5.7	5.7	5.5	5.5	5.6	5.6	5.7	5.7
$h_{c,plen}$	[W/m^{2}K]	3.8	0.7	120.6	1.8	–	–	4.9	1.2	33.2	4.1	–	–
$h_{c,room}$	[W/m^{2}K]	5.4	7.7.	6.6	9.3	9.7	12.6	5.5	8.0	6.4	9.4	9.7	12.8

Table 7
The total, radiant and convective heat transfer in the room for mixing ventilation scenarios. Position 1 and 2 refers to the heat flux sensor positions in Fig. 6.

		M.2.17		M.2.20		M.2.23		M.3.17		M.3.20		M.3.23	
	Position	1	2	1	2	1	2	1	2	1	2	1	2
$Q_{tot,room}/A$	[W/m^2]	−40.4	−46.6	−30.7	−38.6	−26.6	−32.9	−38.6	−45.0	−27.7	−35.8	−24.4	−31.5
$Q_{r,room}/A$	[W/m^2]	−21.8	−21.0	−14.3	−14.9	−8.2	−9.7	−20.3	−19.9	−12.5	−13.2	−7.7	−8.2
$Q_{c,room}/A$	[W/m^2]	−18.6	−25.6	−16.4	−23.7	−18.4	−23.2	−18.3	−25.1	−15.2	−22.7	−16.8	−23.3
$AUST_{room}$		24.2	24.2	25.5	25.5	26.8	26.8	24.0	24.0	25.3	25.3	26.6	26.6
$h_{tot,room}$	[W/m^{2}K]	9.5	11.4	10.2	12.4	10.3	13.0	9.9	11.8	10.5	13.0	12.8	15.8
$h_{r,room}$	[W/m^{2}K]	5.5	5.5	5.6	5.6	5.7	5.7	5.5	5.5	5.6	5.6	5.7	5.7
$h_{c,room}$	[W/m^{2}K]	5.3	7.6	7.3	10.1	11.5	14.6	5.8	8.1	8.2	11.6	15.6	20.0

siderable uncertainty on the transmission loss. In general, the unbalance rate was below 5 %, except for ACRs of 3 and supply temperatures of 23 °C, where the unbalance rate rose to 7–8 %.

As described in section 3.2, the heat transfer coefficient can be calculated in several ways depending on how the heat transfer coefficient should be evaluated. In Table 6 and Table 7, the total heat transfer and the radiant and convective have been calculated. For the steady-state experiments, there are adiabatic conditions in the plenum. Consequently, the temperature difference between the slab and the air in the plenum is close to zero and thus resulting in an unreal heat transfer coefficient. Hence, the radiant and convective heat transfer coefficient was only calculated from the upper and lower side of the radiant ceiling towards the plenum and the room. Heat flux sensors were located in two positions (1 and 2), as illustrated in Fig. 6 and listed in Table 6 and Table 7.

Several studies have proved that the radiant heat transfer coefficient is approximately 5.5 W/m^{2}K [5,47]. The experiments found that the radiant heat transfer coefficients, in general, were smaller in the plenum. This is because 38% of the ceiling was covered with aluminium heat plates with significantly lower emissivity than the rest of the surfaces. Using the weighted emissivity, the radiant heat transfer coefficient was between 4.0–4.4 W/m^{2}K in the plenum and 5.5–5.7 W/m^{2}K in the room.

The convective heat transfer coefficient showed to be inconclusive in the plenum, which was expected with the prevailing adiabatic conditions, where the convective heat transfer coefficient to the room with 2 ACR varied from 5.3-14.6 W/m^{2}K and for 3 ACR varied from 5.5-20.0 W/m^{2}K dependent on the water temperature. For all the cases, the heat transfer coefficient was higher with higher water temperatures.

Because local airflow patterns influence the local heat transfer coefficients, the global heat transfer coefficients are also reported for the different scenarios. In Table 8, numeric values of h_{global} and h_{LMTD} are listed and in Fig. 8, h_{LMTD} and cooling capacity (Q_{cool}) are illustrated as functions of LMTD.

Table 8
Global heat transfer coefficients and effectiveness.

		ACR 2 D.2.17	ACR 3 D.2.20	ACR 2 D.2.23	ACR 3 D.3.17	D.3.20	D.3.23	M.2.17	M.2.20	M.2.23	M.3.17	M.3.20	M.3.23
$T_{water,sup}$	[°C]	17.0	20.2	23.2	17.5	20.2	23.0	17.1	20.3	23.3	17.1	20.7	23.2
$T_{water,ret}$	[°C]	18.8	21.6	24.2	19.2	21.7	24.0	18.7	21.5	24.0	18.7	21.7	24.1
$LMTD_{room}$	[°C]	−6.4	−5.2	−4.4	−5.9	−5.0	−4.2	−6.6	−5.0	−4.0	−6.2	−4.5	−3.5
$T_{s,ceil,r}$	[°C]	20.3	22.9	25.5	20.5	22.8	25.2	20.3	22.9	25.2	20.3	23.0	25.2
h_{global}	[W/m^{2}K]	9.3	8.3	7.1	9.4	8.6	7.1	8.4	8.3	7.2	8.8	8.1	9.5
h_{LMTD}	[W/m^{2}K]	5.9	5.2	4.2	6.0	5.4	4.3	5.3	5.1	4.3	5.5	4.9	5.2

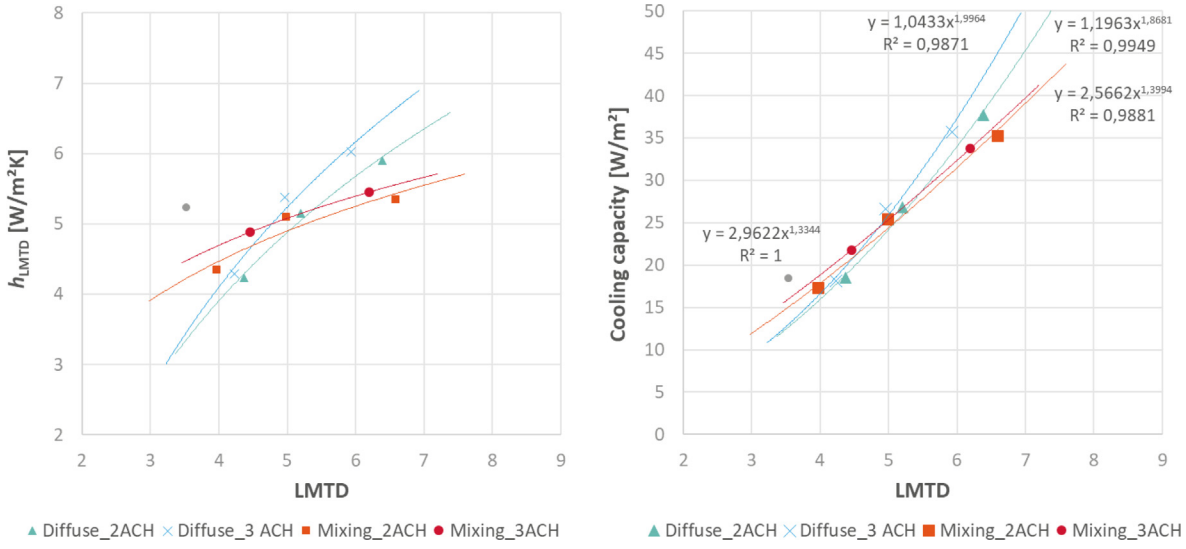

Fig. 8. Left) h_{LMTD} as a function of LMTD. Right) Cooling capacity (Q_{cool}) as a function of LMTD.

The general trend in Table 8, for both diffuse and mixing scenarios, is small increasing heat transfer coefficients when the airflow rates are increased and slightly more significant increases when the water supply temperatures are lowered. The only exception to the trend is the scenario M.3.23 which has the highest heat transfer coefficient.

The global heat transfer coefficient, h_{global}, from Table 8 can be compared to Zhang et al. [16]. Zhang et al. found the global heat transfer coefficient with ventilation rates of 2–4 h^{-1} to be just below 8 W/m^{2}K without diffuse ceiling ventilation and 2–3 W/m^{2}K with the diffuse ceiling. The statement in the introduction was that the suspended ceiling for diffuse ventilation would be a blockage for the heat transfer to the room. This study showed a global heat transfer coefficient of 7.1–9.5 W/m^{2}K, which is on par with the case without the suspended ceiling from Zhang et al.

In Fig. 8 (left), the heat transfer coefficient (h_{LMTD}) for M.3.23 is marked as a greyed-out dot. From the location of other scenarios and the trend lines, it is clear that M.3.23 should be disregarded as an outlier. In Fig. 8 (right), cooling capacity increases with LMTD as expected for both ventilation methods. However, the increase is more significant when using the diffuse ventilation method. The cooling capacity increases with the power of 1.8–2, where the mixing scenarios increase only with the power of 1.1–1.4. The uncertainty for h_{LMTD} is between 0.02–0.05 W/m^{2}K, and the cooling capacity (Q_{cool}) is between 0.1–0.2 W/m^2. The figure shows approx. + 15 % higher cooling capacity for the D.3 scenarios over the M.3 scenarios. If extrapolated the cooling capacity may reach 25% higher values for higher cooling loads (LMTD > 7 K).

4.2. Quasi-steady-state

The steady-state experiments quantified the cooling capacity of the radiant ceiling when combined with diffuse ventilation. However, by steady-state, the plenum surfaces became adiabatic, and the effect of the concrete slab was nullified. This nullification may introduce a significant error because, in practice, the slab can never be in balance. For this reason, quasi-steady-state experiments were conducted in a 24 h cycle to quantify the effect of the slab on the cooling capacity and temperatures in the room. Additionally, the experiments also indicated the amount of thermal energy that can be saved/shifted from day to night and vice versa. Results from both diffuse and mixing scenarios are presented and compared: operative temperature, global heat transfer from water, and local heat flux to quantify the thermal storage of the concrete slab.

For the quasi-steady-state experiments, it was not possible to keep the water temperatures at 17 °C and 23 °C. Consequently, the temperatures were changed to 18 °C and 22 °C, respectively.

The experiments with a water temperature of 18 °C and 20 °C with ACR 3 showed operative temperatures (Fig. 9) below 25.5 °C (Category I) and with ACR 2 below 26 °C (Category II), which indicated thermal comfort in the room. The figure also showed that 22 °C is too high in thermal comfort in a cooling scenario. During the 2x 24 h cycles, it was impossible to keep completely equal conditions, which is why the mixing scenario (M.Q.3) in Fig. 9 actually shows lower operative temperature.

To illustrate the difference in heat transfer, Fig. 10 and Fig. 11 depicts the time-series of heat transfer (Q_w/LMTD) at $T_{w,\,sup}$ = 18 and 20 °C. The heat transfer was calculated for each time step, as

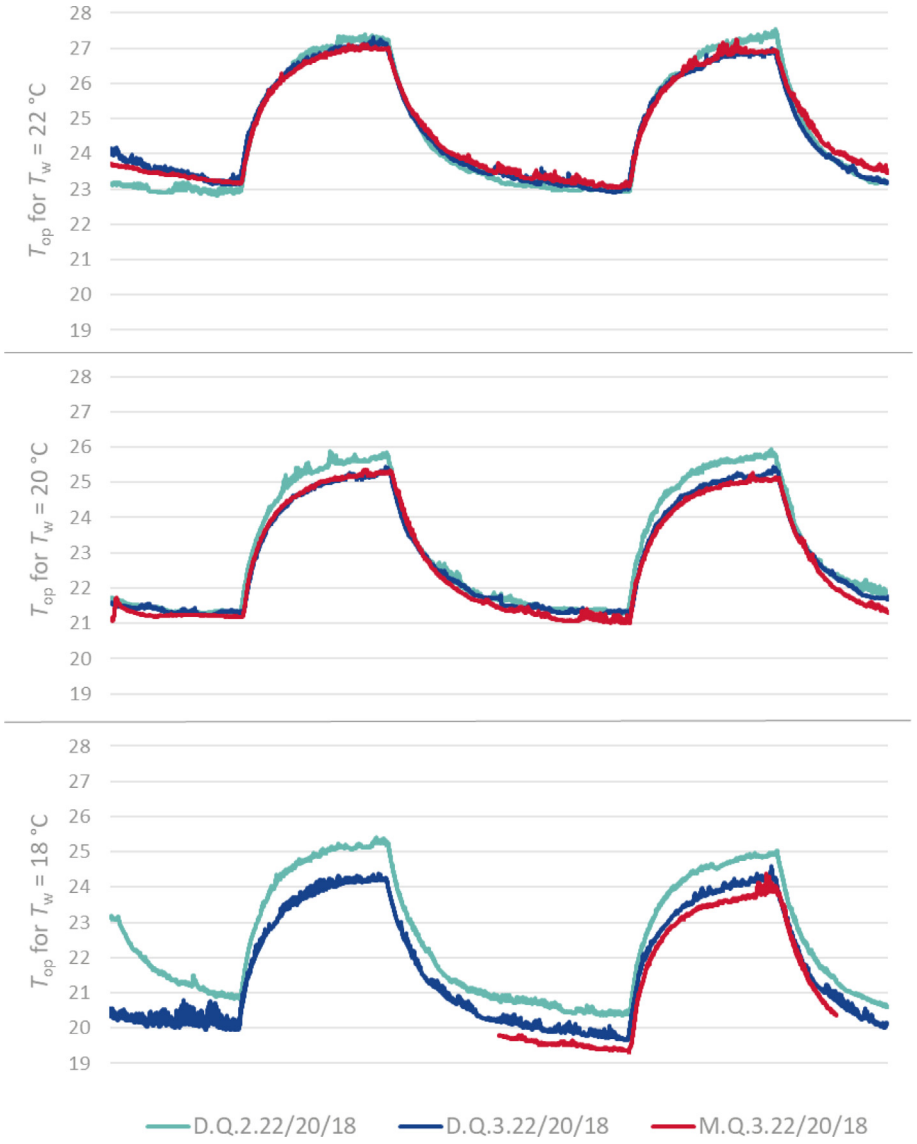

Fig. 9. Operative temperatures in the room for the different scenarios with water temperatures of 22, 20 and 18 °C.

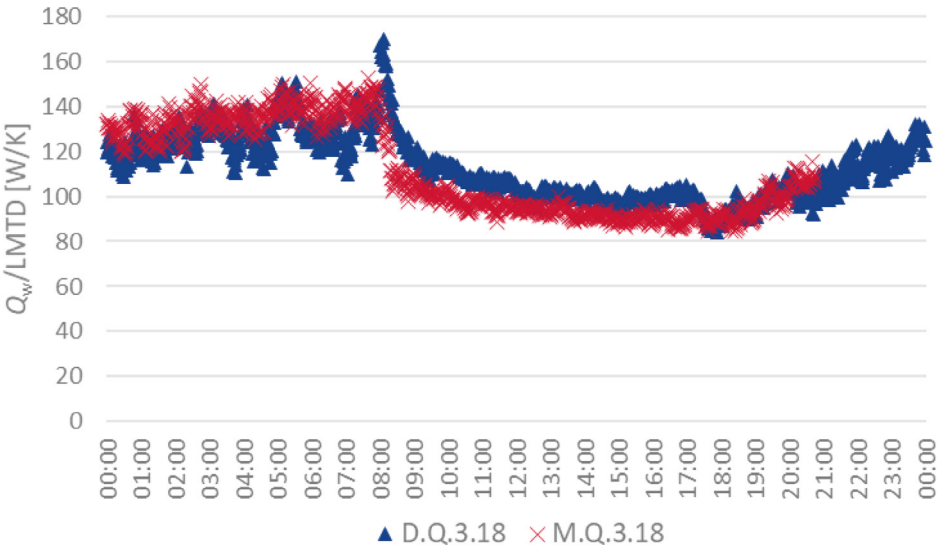

Fig. 10. Heat transfer from water in a 24 h circle with T_w = 18 °C in W/K.

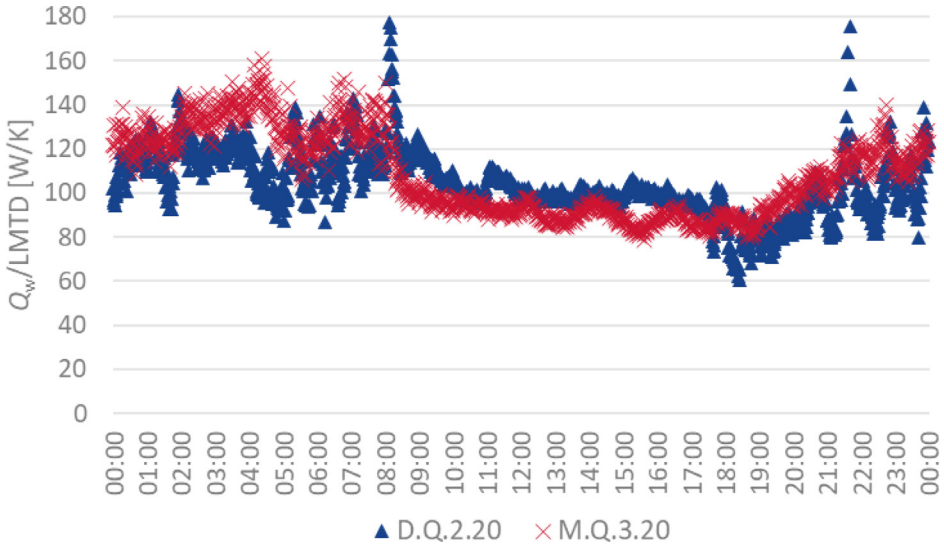

Fig. 11. Heat transfer from water in a 24 h cycle with T_w = 20 °C in W/K.

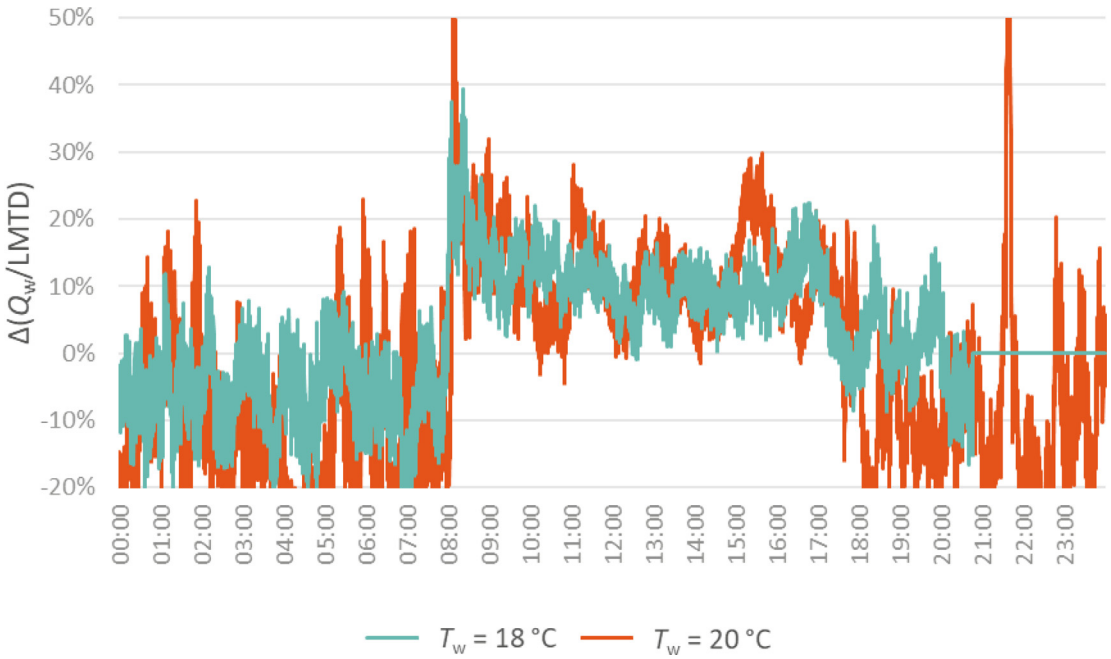

Fig. 12. Increase from mixing to diffuse scenarios in heat transfer for T_w = 18 °C and T_w = 20 °C. Positive values mean heat transfer was higher for diffuse scenario.

it changes during the day with ventilation, internal gains and occupants.

In Fig. 12, a comparison of the diffuse and mixing scenarios is shown for each time step. During the night, the heat transfer for the mixing scenario is 3–9 % higher. During the day, the diffuse scenario is on average 11–12 % higher. Results from T_w = 22 °C scenario is not depicted, because the experiments suffered from adiabatic conditions and therefore unreal results.

Ideally, the heat transfers should be similar at night when the ventilation is turned off and only radiant heat transfer should occur, but as the temperature-series in Fig. 9 illustrate, it was not possible to achieve completely equal conditions in the experiments.

It is difficult to measure the specific effect from the exposed slab, as the heat flux sensor is a local sensor that is accurate for the point where it is placed but conditions can vary in different places in the room. Fig. 13 shows a comparison from experiments with $T_{w,\,sup}$ = 18 °C, where the heat transfer from the slab surface is shown as W/K ($h_{tot,\,slab} \cdot A_{ceil}$; T_{op} in plenum) to compensate for the differences in the two experiments. The time-series show that the slab provides heating in the morning and during the night (which means it is cooling down), but around 11:00 in the diffuse case, the slab starts to absorb heat and cool the plenum, hence helping the radiant ceiling in pre-cooling the ventilation air. The figure shows cooling of approx. 40 W/K from the slab in the afternoon with

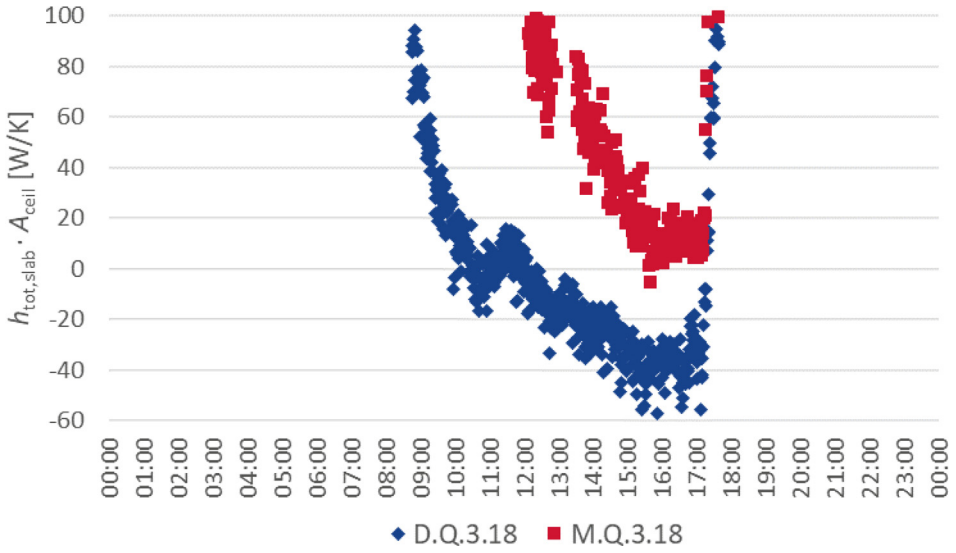

Fig. 13. Heat transfer from slab during a 24 h cycle with T_w = 18 °C in W/K. The figure is zoomed in on 08:00 to 18:00.

ventilation supply $T_{v,sup}$ = 22 °C. The slab can be even more beneficial in a case with higher ventilation supply temperatures, e.g. $T_{v,sup}$ = 28 °C, which would change the additional cooling from the slab to 240 W (= +11 W/m^2).

5. Discussion

The objective was to investigate the HVACeiling concept in a full-scale experimental setup and analyse the cooling performance and the heat transfer both in the plenum and in the room.

5.1. Steady-state

The steady-state experiments showed a difference in cooling capacity, increasing with higher cooling load, which is expected because the advantage of using diffuse ventilation over mixing is to "reuse" cooling from the plenum. The advantage increased with lower ceiling temperature. The steady-state experiments showed that it was possible to achieve thermal comfort.

The radiant heat transfer coefficient in the steady-state experiments showed to be on par with literature in the room and the plenum when the emissivity of the aluminium plates on the ceiling top was included.

The ratio of ceiling output to total cooling output was in the range 0.40–0.85 across scenarios and according to Rehva Guidebook 01 [27] this system should behave like a mixing system.

The amount of mixing in both diffuse and mixing scenarios seemed to be similar due to equal inclination of the temperature gradients, but the gradients also disclosed that some stratification was present which was probably due to the concentration of strong heat sources at one end of the room.

In the steady-state experiments, the slab became adiabatic, and therefore, it was impossible to conclude on the heat transfer coefficients from the slab. In general, the minor temperature differences in some of the experiments caused problems, notably in scenario M.3.23, which was altogether disregarded. The thermal balance of the experiments was acceptable, and uncertainty was also low due to meticulous calibration (0.1–0.2 W/m^2 in Fig. 8, right). This means it is acceptable to somewhat extrapolate for LMTD > 6, but more experiments with higher cooling loads (and therefore higher LMTD), should be conducted to validate the extrapolation.

5.2. Quasi-steady-state

The results did not show any difference on the T_{op}, but the cooling capacity was measured to be up to 12 % higher in combination mode. The reason for not measuring an impact on T_{op} was due to variable conditions. However, the effect of 12 % more cooling capacity on the operative temperature can be calculated by setting up a simple heat balance equation and solve for the resulting operative temperature. In this manner, the extra cooling capacity of 12 % translates into a temperature drop of 0.5 °C, all other things equal.

The quasi-steady state did not show much positive influence on the cooling capacity (40 W/K) from the thermal mass in the concrete slab, which is congruent with simulation results [2], that stipulated only minor cooling advantages of 2 %, almost immeasurable. The ventilation supply temperature must be significantly higher than the slab (T > 28 °C) to show the significant advantages of the increased thermal mass. Then a cooling increase of 10 % could be expected.

5.3. Experimental setup

Due to the experimental facilities, the water flow rates varied slightly. The intended water flow rate was 300 kg/h to the manifold (100 kg/h in each circuit). However, this varied through the experiments with an average water flow rate of 302 kg/h ± 7 %.

The radiant ceiling tile assembly was not perfect and with air gaps as the glue of the assembling aluminium profiles had loosened some places. Consequently, conduction from the pipes to the heat distribution plate and the room was limited for some ceiling tiles. If the ceiling tile were assembled without air gaps, the heat transfer and heat transfer coefficient might have been higher.

The operative room sensor at 1.1 m height was measuring slightly higher temperature than the air temperature sensor in the same location, which is counter-intuitive considering the ceiling is chilled. But this was probably due to a combination of the ceiling being only slightly colder than the air, the radiative-to-convective ratio of the heat resistant film on the wall and the thermal dummies and the view factors between sensor and heat sources.

5.4. Moisture

The experimental investigation did not include any measurements of humidity. Overall the moisture-related issues in the

plenum are reduced when the water supply temperature is close to the room temperature. The experiments were carried out in a Danish testing facility, and in the Danish climate, the dew point temperature rises above the water temperature for only short periods of time. In practice and in a broader European context with warmer and more humid climates, it is necessary to include a cooling coil as part of the air handling unit, which would centrally dehumidify the air before it enters the plenum.

5.5. Design practice

The reported results may be transformed into design advice in the following way. The ventilation rate should be enough to cover the atmospheric air quality criteria and be supplied to the plenum via an air handling unit with a cooling coil. The coil cools the ambient air to 22 °C and in the process dehumidifies the air. The ceiling is supplied with water at 18 °C and both the cooling coil and ceiling may be connected to the same source. The cooling output would be 12% higher and the operative temperature 0.5 °C lower. If the ambient air rises above 22 °C, and there is no need for dehumidification, then the extra cooling output from the slab storage seems to cover the additional ventilative heat load, but this should be investigated in more detail.

6. Conclusions

The objectives of this experimental work were to quantify the effect on heat transfer when a radiant ceiling is combined with diffuse ventilation and quantify the extra thermal cooling storage of the slab in the combination mode. Therefore, steady-state and quasi-steady-state experiments were conducted in a climate chamber.

The steady-state experiments showed a maximum increase in cooling capacity with diffuse ventilation of 15 %, pointing towards 25 % if extrapolated. The quasi-steady-state experiments showed an increase of cooling output on average over the day (occupancy) of 12 % with diffuse ventilation. This can be translated into 0.5 °C cooler indoor temperature. The benefit from the exposed slab was challenging to measure when the ventilation supply temperature (=ambient temperature) was only 22 °C; however, up to 11 W/m^2 extra cooling capacity could be expected for warmer summer days of 28 °C ambient temperature.

Declaration of Competing Interest

The authors declare that they have no known competing financial interests or personal relationships that could have appeared to influence the work reported in this paper.

Acknowledgements

We would like to acknowledge the financial help from Saint-Gobain Nordic A/S and Innovation Fund Denmark, grant 5189-00088A that made this study possible. We declare that neither funding bodies had any influence nor attempted to gain influence on the analyses, results and/or conclusions of this study at any time or in any way.

References

[1] Clean energy for all Europeans package | Energy, Eur. Commesion. (n.d.). https://ec.europa.eu/energy/topics/energy-strategy/clean-energy-all-europeans_da (accessed October 26, 2020).
[2] M.R. Krusaa, C.A. Hviid, Combining suspended radiant ceiling with diffuse ventilation – numerical performance analysis of low-energy office space in a temperate climate, J. Build. Eng. 38 (2021), https://doi.org/10.1016/j.jobe.2021.102161.
[3] M.R. Krusaa, C.A. Hviid, Reduced-scale experiments of heat transfer from integrated radiant ceiling panel and diffuse ceiling ventilation, Appl. Therm. Eng. 197 (2021), https://doi.org/10.1016/J.APPLTHERMALENG.2021.117348 117348.
[4] S. Lestinen, P. Mustakallio, S. Kilpeläinen, R. Kosonen, J. Jokisalo, H. Koskela, A. K. Melikov, Experimental comparison of thermal conditions in office rooms: Diffuse ceiling ventilation, chilled beam system, and chilled ceiling combined with mixing ventilation, Sci. Technol. Built Environ. 26 (2020) 631–642, https://doi.org/10.1080/23744731.2019.1708210.
[5] J. Babiak, B.W. Olesen, D. Petras, Low Temperature Heating and High Temperature Cooling: REHVA Guidebook no. 7, 2013.
[6] C. Zhang, T. Yu, P. Heiselberg, M. Pominaowski, P. Nielsen, Diffuse Ceiling Ventilation – Design Guide, DCE, Tech. Rep. 10.13140/RG.2.2.25455.43684 (2016).
[7] C.A. Hviid, S. Svendsen, Experimental study of perforated suspended ceilings as diffuse ventilation air inlets, Energy Build. 56 (2013) 160–168, https://doi.org/10.1016/j.enbuild.2012.09.010.
[8] W. Wu, Z. Tong, N. Yoon, Y. Chen, Y. Lv, T. Ærenlund, J. Benner, Diffuse ceiling ventilation for buildings: A review of fundamental theories and research methodologies, J. Clean. Prod. 211 (2019), https://doi.org/10.1016/j.jclepro.2018.11.148.
[9] R. Guo, P. Heiselberg, Y. Hu, H. Johra, C. Zhang, R.L. Jensen, K.T. Jønsson, P. Peng, Experimental investigation of convective heat transfer for night cooling with diffuse ceiling ventilation, Build. Environ. 193 (2021), https://doi.org/10.1016/j.buildenv.2021.107665.
[10] R. Li, T. Yoshidomi, R. Ooka, B.W. Olesen, Field evaluation of performance of radiant heating/cooling ceiling panel system, Energy Build. 86 (2015) 58–65, https://doi.org/10.1016/j.enbuild.2014.09.070.
[11] H. Tario, D. Schmidt, Annex 49 -, Summary report (2011). http://www.annex49.info/download/summary_report.pdf.
[12] W. Shan, D. Rim, Thermal and ventilation performance of combined passive chilled beam and displacement ventilation systems, Energy Build. (2018), https://doi.org/10.1016/j.enbuild.2017.10.010.
[13] P. Filipsson, A. Trüschel, J. Gräslund, J.O. Dalenbäck, Performance evaluation of a direct ground-coupled self-regulating active chilled beam system, Energy Build. 209 (2020), https://doi.org/10.1016/j.enbuild.2019.109691.
[14] P. Filipsson, A. Trüschel, J. Gräslund, J.-O. Dalenbäck, Modelling of rooms with active chilled beams, J. Build. Perform. Simul. 2020 (2020) 409–418, https://doi.org/10.1080/19401493.2020.1752801.
[15] T. Yu, P. Heiselberg, B. Lei, M. Pomianowski, C. Zhang, R. Jensen, Experimental investigation of cooling performance of a novel HVAC system combining natural ventilation with diffuse ceiling inlet and TABS, Energy Build. 105 (2015) 165–177, https://doi.org/10.1016/j.enbuild.2015.07.039.
[16] C. Zhang, P.K. Heiselberg, M. Pomianowski, T. Yu, R.L. Jensen, Experimental study of diffuse ceiling ventilation coupled with a thermally activated building construction in an office room, Energy Build. 105 (2015) 60–70, https://doi.org/10.1016/j.enbuild.2015.07.048.
[17] C. Zhang, P.K. Heiselberg, Q. Chen, M. Pomianowski, Numerical analysis of diffuse ceiling ventilation and its integration with a radiant ceiling system, Build. Simul. 10 (2017) 203–218, https://doi.org/10.1007/s12273-016-0318-z.
[18] M.R. Krusaa, C.A. Hviid, J. Kolarik, Numerical analysis of the potential of using light radiant ceilings in combination with diffuse ventilation to achieve thermal comfort in NZEB buildings, in: 38th AIVC Conf., Nottingham, 2017.
[19] N. Langner, D. Bewersdorff, Thermal and acoustical simulation of open space working areas in commercial buildings equipped with thermally activated building systems, in: 14th Int. Conf. Int. Build. Perform. Simul. Assoc., Hyderabad, India, 2015: pp. 736–742.
[20] G. Frenger, Heating and ventilation system, 2718383, 1955.
[21] B. Kilkis, A. Manas, Composite hybrid panel, or building element for combined heating, cooling, ventilating and air-conditioning, 2008.
[22] Plafotherm® DS AirHybrid | Lindner Group, (n.d.). https://www.lindner-group.com/en/fit-out-products/heated-and-chilled-ceilings/heated-and-chilled-hybrid-ceilings/plafothermr-ds-airhybrid/# (accessed March 5, 2021).
[23] C. Karmann, F. Bauman, P. Raftery, S. Schiavon, M. Koupriyanov, Effect of acoustical clouds coverage and air movement on radiant chilled ceiling cooling capacity, Energy Build. 158 (2018) 939–949, https://doi.org/10.1016/j.enbuild.2017.10.046.
[24] Paul Raftery, D. Douglass-Jaimes, Ceiling Fan Design Guide, (2020).
[25] Thermisch aktive Kühlsegel und Hezdeckensegel von CLIMALINE, (n.d.). https://climaline-gmbh.com/2019/11/17/climaline-hybridair/ (accessed March 5, 2021).
[26] Thermo Panel 4T - Die Modulare - Kühldecke Funktion, (n.d.). https://climaline-gmbh.com/produkte/thermo-panel-4t/ (accessed July 20, 2021).
[27] H. Skistad, E. Mundt, P.V. Nielsen, K. Hagstrøm, J. Railio, Displacement Ventilation in Non-industrial Premises (2002).
[28] ISO 17772-2, Energy performance of buildings — Overall energy performance assessment procedures — Part 2: Guideline for using indoor environmental input parameters for the design and assessment of energy performance of buildings, 2018.
[29] DS/EN 16798-3, Energy performance of buildings - Ventilation for buildings - Part 3: For non-residential buildings - Performance requirements for ventilation and room conditioning systems, (2017).
[30] P. Weitzmann, Modelling building integated heating and cooling systems, 2004. Technical University of Denmark, BYG-Report, No. R-091.

[31] A. Simone, J. Babiak, M. Bullo, G. Landkilde, B.W. Olesen, Operative temperature control of radiant surface heating and cooling systems, Proc. Indoor Air 2007 (2) (2007) 1–8. http://www.irbnet.de/daten/iconda/CIB8368.pdf.
[32] HF-10S Heat flux sensor | EKO Instruments, (n.d.). https://eko-eu.com/products/material-analysis/heat-flux-sensors/hf-10s-heat-flux-sensor?fbclid=IwAR1ohIWkvFLuj323VtUiYJmYsj5CFFWd2m7nKRkvsqHDXSgyQ6j-Fhc5KnM (accessed March 5, 2021).
[33] Electrolube, HTS, (n.d.). https://electrolube.com/wp-content/uploads/2019/09/HTS.pdf (accessed March 5, 2021).
[34] R. Onsberg, M.S. Eriksen, Investigations and development of capillary thermal ceiling systems with integrated ventilation, Technical University of Denmark (DTU), 2014.
[35] F. Causone, S.P. Corgnati, M. Filippi, B.W. Olesen, Experimental evaluation of heat transfer coefficients between radiant ceiling and room, Energy Build. 41 (2009) 622–628, https://doi.org/10.1016/j.enbuild.2009.01.004.
[36] A.J.N. Khalifa, Natural convective heat transfer coefficient - a review I. Isolated vertical and horizontal surfaces, Energy Convers. Manag. 42 (2001) 491–504, https://doi.org/10.1016/S0196-8904(00)00042-X.
[37] H.B. Awbi, Calculation of convective heat transfer coefficients of room surfaces for natural convection, Energy Build. 28 (1998) 219–227, https://doi.org/10.1016/s0378-7788(98)00022-x.
[38] T. Cholewa, M. Rosiński, Z. Spik, M.R. Dudzińska, A. Siuta-Olcha, On the heat transfer coefficients between heated/cooled radiant floor and room, Energy Build. 66 (2013) 599–606, https://doi.org/10.1016/j.enbuild.2013.07.065.
[39] H.B. Awbi, A. Hatton, Mixed convection from heated room surfaces, Energy Build. 32 (2000) 153–166, https://doi.org/10.1016/S0098-8472(99)00063-5.
[40] J.W. Jeong, S.A. Mumma, Ceiling radiant cooling panel capacity enhanced by mixed convection in mechanically ventilated spaces, Appl. Therm. Eng. 23 (2003) 2293–2306, https://doi.org/10.1016/S1359-4311(03)00211-4.
[41] M. Andrés-Chicote, A. Tejero-González, E. Velasco-Gómez, F.J. Rey-Martínez, Experimental study on the cooling capacity of a radiant cooled ceiling system, Energy Build. 54 (2012) 207–214, https://doi.org/10.1016/j.enbuild.2012.07.043.
[42] B.W. Olesen, E. Michel, F. Bonnefoi, M. De Carli, Heat exchange coefficient between floor surface and space by floor cooling - theory or a question of definition, ASHRAE Trans. 106 (2000) 684–694.
[43] T. Cholewa, R. Anasiewicz, A. Siuta-Olcha, M.A. Skwarczynski, On the heat transfer coefficients between heated/cooled radiant ceiling and room, Appl. Therm. Eng. 117 (2017) 76–84, https://doi.org/10.1016/j.applthermaleng.2017.02.019.
[44] H.B. Awbi, A. Hatton, Natural convection from heated room surfaces, Energy Build. 30 (1999) 233–244, https://doi.org/10.1016/S0378-7788(99)00004-3.
[45] A.J.N. Khalifa, R.H. Marshall, Validation of heat transfer coefficients on interior building surfaces using a real-sized indoor test cell, Int. J. Heat Mass Transf. 33 (1990) 2219–2236, https://doi.org/10.1016/0017-9310(90)90122-B.
[46] A.J.N. Khalifa, Natural convective heat transfer coefficient - a review II. Surfaces in two- and three-dimensional enclosures, Energy Convers. Manag. 42 (2001) 505–517, https://doi.org/10.1016/S0196-8904(00)00043-1.
[47] J. Shinoda, O.B. Kazanci, S.-I. Tanabe, B.W. Olesen, A review of the surface heat transfer coefficients of radiant heating and cooling systems, Build. Environ. 159 (2019), https://doi.org/10.1016/j.buildenv.2019.05.034.
[48] S. Bell, Measurement good practice guide, Phys. Lab. No. 11 (2004) 1–41, https://doi.org/10.1111/j.1468-3148.2007.00360.x.
[49] ISO 17772-1, Energy performance of buildings – Indoor environmental quality – Part 1: Indoor environmental input parameters for the design and assessment of energy performance of buildings, 2017.